

A Spatiotemporal, Patient Individualized Simulation Model of Solid Tumor Response to Chemotherapy *in Vivo*: The Paradigm of Glioblastoma Multiforme Treated by Temozolomide

Georgios S. Stamatakos*, Vassilis P. Antipas, *Student Member, IEEE*, and Nikolaos K. Uzunoglu, *Fellow, IEEE*

Abstract—A novel four-dimensional, patient-specific Monte Carlo simulation model of solid tumor response to chemotherapeutic treatment *in vivo* is presented. The special case of glioblastoma multiforme treated by temozolomide is addressed as a simulation paradigm. Nevertheless, a considerable number of the involved algorithms are generally applicable. The model is based on the patient's imaging, histopathologic and genetic data. For a given drug administration schedule lying within acceptable toxicity boundaries, the concentration of the prodrug and its metabolites within the tumor is calculated as a function of time based on the drug pharmacokinetics. A discretization mesh is superimposed upon the anatomical region of interest and within each geometrical cell of the mesh the most prominent biological "laws" (cell cycling, necrosis, apoptosis, mechanical restrictions, etc.) are applied. The biological cell fates are predicted based on the drug pharmacodynamics. The outcome of the simulation is a prediction of the spatiotemporal activity of the entire tumor and is virtual reality visualized. A good qualitative agreement of the model's predictions with clinical experience supports the applicability of the approach. The proposed model primarily aims at providing a platform for performing patient individualized *in silico* experiments as a means of chemotherapeutic treatment optimization.

Index Terms—Cancer, chemotherapy, chemotherapy optimization, glioblastoma multiforme, *in silico* oncology, Monte Carlo, neovasculature, patient individualized optimization, temozolomide, Temodal™, Temodar™, tumor growth, simulation model.

I. INTRODUCTION

ANALYTICAL description of tumor growth and response to several therapeutic modalities such as radiation therapy and chemotherapy has received considerable attention during the last decades. Examples of the efforts concerning modeling

Manuscript received January 28, 2005; revised January 29, 2006. This work was supported in part by the Hellenic Ministry of Education and Religious Affairs under the program: "Herakleitos: Fellowships for Research of the National Technical University of Athens" and in part by the European Union. *Asterisk indicates corresponding author.*

*G. S. Stamatakos is with the National Technical University of Athens, School of Electrical and Computer Engineering, Institute of Communication and Computer Systems, Laboratory of Microwaves and Fiber Optics, *In Silico* Oncology Group, 9, Iroon Polytechniou, GR-157 80 Zografos, Greece (e-mail: gestam@central.ntua.gr).

V. P. Antipas and N.K.Uzunoglu are with the National Technical University of Athens, School of Electrical and Computer Engineering, Institute of Communication and Computer Systems, Laboratory of Microwaves and Fiber Optics, *In Silico* Oncology Group, GR-157 80 Zografos, Greece (e-mail: van-tipas@gmail.com; nnap@otenet.gr).

Digital Object Identifier 10.1109/TBME.2006.873761

of the tumor response to chemotherapy include the following. Chuang [1] presented a theoretical study of pharmacokinetic and cell kinetic models for cancer chemotherapeutic systems. In his approach, pharmacokinetic models and cell-drug interactions at the tumor site are incorporated into the cell cycle kinetic models to form the cancer chemotherapeutic model systems. Levin *et al.* [2] defined specific factors that they believed to be of primary importance in drug delivery to brain tumors, and, using computer simulation they modeled their effects. Ozawa *et al.* [3] presented a pharmacodynamic model for the cell cycle phase-specific antitumor agents as well as for the cell cycle phase-nonspecific agents. Jean *et al.* [4] developed an educational computer-based program simulating experiments of anti-tumor activity. The input of the program includes the dose, the number of treatments/day, the total number of treatments and the time interval between the treatments. Nani and Oguztoereli [5] presented a set of mathematical models and computer simulations of the response of haematological and gynaecological tumors to chemotherapy. To optimize chemotherapeutic treatment Iliadis and Barbolosi [6], [7] developed an analytical model describing the pharmacokinetics of anticancer drugs, antitumor efficacy and drug toxicity. Davis and Tannock [8] modeled the effect of repopulation of tumor cells between cycles of chemotherapy. Gardner [9] developed a computer model, the kinetically tailored treatment or KITT model, to predict drug combinations, doses, and schedules likely to be effective in reducing tumor size and prolonged patient life. Ward and King [10] adapted an avascular tumor growth model to compare the effects of drug application on multicell spheroids and on monolayer cultures. From the above brief literature account it appears that although extensive efforts have been made towards modeling chemotherapy response in a generic setting, no simulation models referring to the individual patient's imaging [exact three-dimensional (3-D) geometry] and other pertinent data have been published as yet. To respond to such a need a novel four-dimensional (4-D) , patient-specific Monte Carlo simulation model of solid tumor response to chemotherapeutic treatment *in vivo* is presented in this paper. The special case of glioblastoma multiforme treated by the alkylating agent temozolomide is addressed although a considerable number of the involved algorithms are generally applicable. The model is based on the patient's imaging, histopathologic and pharmacodynamic/genetic data and primarily aims at providing a reliable platform for performing

patient individualized *in silico* (on the computer) experiments as a means of chemotherapeutic treatment optimization.

II. DATA COLLECTION

The imaging data [e.g., T1 contrast enhanced magnetic resonance imaging (MRI), positron emission tomography (PET) slices, possibly fused] including the delineation of the (glioblastoma multiforme) tumor and its necrotic area as well as the adjacent anatomical structures of interest, the histopathologic (e.g., type of tumor) and eventually the genetic data (e.g., DNA microarray output appropriately interpreted through a pertinent genetic network) of the specific tumor, are collected. It is pointed out that the imaging data (e.g., T1 contrast enhanced MRI) provide information on 1) the boundaries of the gross volume of the tumor, 2) the volume itself, and 3) the spatial distribution of the metabolic activity of the tumor (regions where there is significant provision of oxygen and nutrients through the neovasculature, and “necrotic” regions where there is lack of adequate vascularization and subsequently lack of adequate oxygenation and provision of nutrients).

Concerning the delineation and extraction of the tumor, the following procedures take place. A specialized clinician delineates the structures of interest, i.e., the necrotic and the well vascularized areas of the tumor on each tomographic (e.g., MRI) slice available using a dedicated software tool previously developed by our research group. The imaging data under consideration can be either digital tomograms in DICOM format or the scanning output of conventional films (e.g., in TIFF format). Manual segmentation obviously relies on the user’s clinical experience and training. Each user defined slice contour consists of a number of ordered points which appear on a screen window through the use of the mouse. There are possibilities of addition, translation or removal of the contour points. A simple trilinear interpolation is used as a first approximation in order to substitute the missing information due to the generally varying spatial interval between subsequent slices. In this way the value of each interpolated element is calculated based on the weighted values of its six neighboring elements. It is assumed that the color density varies linearly along the three basic axes between the two closest image elements that lie at both sides of the element under consideration. Shape-based interpolation through the use of distance maps (6-neighbor distance transformation) is applied to the delineation contours in order to acquire resolution equal to the resolution of the imaging data following interpolation. Improved interpolation techniques can also be used.

Contrast enhanced T1 MRI images usually provide sharp edges between the hyperintense and hypointense regions of the tumor. Poorly differentiated glioblastoma multiforme cells when lying in the vicinity of functional capillaries that provide them with sufficient oxygen and nutrients are expected to be cell cycling most of the time unless spontaneous apoptosis or a therapeutic effect is taking place (e.g., cytostasis and subsequent apoptosis due to temozolomide action). Tumor cells lying at a large distance from their nearest neovasculature capillaries will either be in the G0 phase or the necrotic one due to inadequate oxygenation and nutrition. Within a given geometrical cell, the distribution of the proliferating tumor cells throughout the cell cycle phases is performed in a statistical way based on the mean duration of each separate phase.

Concerning handling of the imaging data, although this paper does not focus on the techniques that can be used in order to perform image segmentation, automatic segmentation might be a better alternative to the manual one adopted so far. To this end techniques such as the ones appearing in [11] and [12] can be used. It is pointed out that at the present phase of the model development a perfect segmentation is not absolutely necessary. This is because uncertainties in the estimation of specific biological parameters would prevent full exploitation of a perfect segmentation.

The imaging information is introduced into the 3-D visualization package (AVS-Express™), which performs the visualization of both the tumor and its surrounding region by combining volume and surface rendering techniques. Especially for the case of glioblastoma multiforme, gadolinium-enhanced T1-weighted images have been mainly considered by our group up to now. According to [13], the hyper-intense, white region of the tumor reflects an area of extensive blood-brain/tumor barrier leakage. Since this regional neovascular setting provides tumor cells with sufficient nutrition, this region contains the highly metabolizing and, therefore, the highly proliferating, e.g., dividing tumor cells. It is also pointed out that up to now no work has been published in which direct exploitation of the actual 3-D structural and functional information provided by imaging techniques is used in order to optimize chemotherapy on a patient-specific level. Undoubtedly tumor cells infiltrate into the brain well beyond the imaged edge of the tumor and infiltrations play a critical role in patient survival. Extensive work on this aspect of glioblastoma has been done by Swanson *et al.* [14], [15]. Nevertheless, control of the main imageable tumor which is addressed in this paper is a straightforward necessity.

III. BIOLOGICAL AND CLINICAL BACKGROUND

A. Tumor Growth and Chemotherapeutic Treatment Biology

The cytokinetic model shown in Fig. 1 is proposed and adopted. According to this model, a tumor cell when cycling passes through the phases G1 (gap 1), S (DNA synthesis), G2 (gap 2), and M (mitosis) [16]–[19]. After mitosis is completed, each one of the resulting cells re-enters G1 if oxygen and nutrient supply in its current position is adequate. Otherwise, it enters the resting G0 phase in which if oxygen and nutrient supply are inadequate it can stay for a limited time (T_{G0}). Subsequently, it enters the necrotic phase which leads to cell death unless the local environment of the cell becomes adequate before the expiration of T_{G0} . In the latter case, the cell re-enters G1. In addition to the previously described pathway, there is always a chance that each cell residing in any phase—other than necrosis or apoptosis—dies with some probability/hour due to ageing and spontaneous apoptosis. This probability represents the cell loss rate due to apoptosis and is the product of the cell loss factor due to apoptosis and the cell birth rate [20]. The cell birth rate can be considered as the ratio of the growth fraction to the cell cycle duration [20]. A rather analogous approach to the cytokinetic modeling of tumor cells for the case of non-Hodgkin lymphomas has been adopted by Ribba *et al.* [21]. Side effects, immunologic reactions, formation of metastases, and drug resistance as a phenomenon building up with time are neglected in the current version of

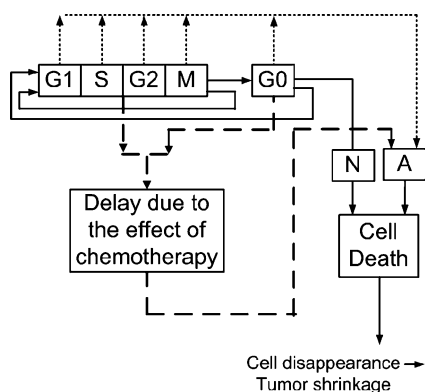


Fig. 1. A simplified cytokinetic model of a tumor cell. Symbol explanation. G1: G1 phase; S: DNA synthesis phase; G2: G2 phase; G0: G0 phase; N: necrosis; A: apoptosis. The cytotoxicity produced by TMZ is primarily modeled by a delay in the S phase compartment (TDS) (“Delay due to the effect of chemotherapy” in the diagram) and subsequent apoptosis. The delay box simply represents the time corresponding to at most two cell divisions being required before the emergence of temozolomide cytotoxicity. It is not a time interval additional to the times represented by the cell cycle phase boxes.

the model. Only the tomographically visible gross volume of the tumor is taken into account at this stage of the simulation model development process. The response of the entire clinical tumor, the surrounding edema and the whole body reactions to the chemotherapeutic scheme are to be addressed in a future version.

Based upon the experimental observation that the diffusion limit of oxygen is about 100 μm from the capillaries and that there is usually progressive hypoxia from the outer tumor layer to the center of the tumor [22]–[27], an intermediate “G0 layer” (containing a substantial number of hypoxic cells) is considered. During the tumor growth process, new capillaries are assumed to emerge. In this way both the tumor volume characterized by pronounced metabolic activity in the beginning of the simulated period and the volume subsequently added to the tumor are considered to be able to sustain proliferation.

In the case of chemotherapeutic treatment with the pro-drug temozolomide (TMZ) with the chemical name 3,4-dihydro-3-methyl-4-oxoimidazo[5,1-d]-as-tetrazine-8-carboxamide, a given proliferating or dormant cancer cell may or may not be affected by the treatment [28]–[30]. In the former case, the methyldiazonium ion methylates guanine residues in the DNA molecules [28]. The resulting interruptions in the daughter strands are inhibitory to replication in the subsequent S-phase and account for up to two cell divisions being required before the emergence of Temozolomide cytotoxicity [29]. Thus, the effect of TMZ is simulated by both a time delay TDS in the S phase (“Delay due to the effect of chemotherapy” in Fig. 1) taken equal to 11/2 of the cell cycle duration. After expiration of TDS, affected cells are assumed to proceed to death via the apoptotic pathway. It should be noted that certain investigators assume that affected cells are arrested at the G2/M checkpoint before undergoing apoptosis [30]. Nevertheless, no essential difference from the computing point of view would arise in case that such an assumption were more realistic than the one adopted, as the only difference between the two approaches lies in a rather insignificant time delay.

B. Temozolomide Pharmacokinetics and Pharmacodynamics

TMZ belongs to a new class of alkylating agents known as imidazotetrazines. TMZ is a small molecule with a molecular weight of 194 daltons and is, therefore, readily absorbed in the digestive tract and, because it is lipophilic, it is able to cross the blood-brain barrier. TMZ is robustly stable at the acidic pH of the stomach. However, once in contact with the slightly basic pH of the blood and tissues, TMZ spontaneously undergoes hydrolysis to the active metabolite 5-(3-methyltriazen-1-yl)imidazole-4-carboxamide (MTIC), which rapidly breaks down to form the reactive methyldiazonium ion [30]. The methyldiazonium ion formed by the breakdown of MTIC primarily methylates guanine residues in the DNA molecule, resulting in the formation of O^6 - and N^7 -methylguanine. The formation of O^6 -methylguanine is primarily responsible for the cytotoxic effects of TMZ and DTIC. When DNA mismatch repair enzymes attempt to excise O^6 -methylguanine, they generate single- and double-strand breaks in the DNA, leading to activation of apoptotic pathways [28]–[47]. It is pointed out that apoptosis is by far the main way through which cells treated by temozolomide die [30], [47]. It is also stressed that although the cytotoxicity of TMZ is due to its decomposition products, both its pharmacokinetics and pharmacodynamics are referred to the parent drug concentration [38].

TMZ pharmacokinetics can be adequately described by a one compartment open model [30]. The absorption process for oral drug administration can be described by a first order differential equation [34]–[37], [47]–[50]. The plasma concentration is given by

$$C_p = \frac{F \cdot D \cdot k_a}{V_d \cdot (k_a - k_{el})} (e^{-k_{el} \cdot t} - e^{-k_a \cdot t}) \quad (1)$$

where D stands for the administered dose/fraction, F for the bioavailability (the fraction of drug reaching the systemic circulation following administration by any route), and V_d for the volume of distribution. The variable t represents the time elapsed since the drug administration. It is noted that the dose/fraction and the volume of distribution should be adjusted for the actual weight of the patient (e.g., 70 kg). k_a denotes the absorption rate constant whereas k_{el} the elimination rate constant. Both k_a and k_{el} depend on the specific chemotherapy agent and the administered dose/fraction.

The k_a and k_{el} pharmacokinetics parameters have been calculated based on data included in the corresponding study in [38] that has been conducted by the Schering-Plough Research Institute. The values of pharmacokinetics parameters of TMZ in plasma have been measured in patients with advanced cancer. In the present paper the dose values (in milligrams of TMZ/ m^2 of the patient’s body surface) of 150 mg/m^2 , 200 mg/m^2 , and 250 mg/m^2 have been considered [38], [39]. Two oral drug administration schedules have been simulated (see Section VI): the standard one (once a day, for 5 consecutive days/28-day treatment cycle) [37]–[39] and a hypothetical one in which the chemotherapy fractions are distributed more uniformly throughout the 28-day chemotherapy cycle. In the latter scheme more time for the normal tissues to recover between chemotherapy sessions is allowed. The pharmacokinetics constants have been calculated for the three previously mentioned

doses using the method of “residuals.” For the dose of 150 mg/m² the pharmacokinetics constants have been calculated to be $k_a = 3.10 \text{ h}^{-1}$ and $k_{el} = 0.33 \text{ h}^{-1}$, for the dose of 200 mg/m² $k_a = 3.60 \text{ h}^{-1}$ and $k_{el} = 0.39 \text{ h}^{-1}$ and for the dose of 250 mg/m² $k_a = 4.60 \text{ h}^{-1}$ and $k_{el} = 0.74 \text{ h}^{-1}$. The volume of distribution for an individual weighting 70 kg has been taken equal to 28 L (0.4 L/kg [38]). In order to validate the implementation of the calculation method adopted, the plasma concentration for the three doses considered has been “re-calculated” based on the previously estimated values of k_a and k_{el} . The “re-calculated” plasma concentration values have been compared with data included in [38] and an excellent agreement has been observed. The bioavailability of TMZ is practically 1.0 (or 100%) [38].

Being an alkylating agent TMZ belongs to the Cell Cycle Nonspecific Agents (CCNS) [35], [36], [48]–[58]. The Survival Fraction (SF) for the CCNS depends on the following factors [3], [56]–[58]: 1) Average plasma concentration (C_{pav}) of TMZ; 2) Exposure of tumor cells to TMZ (T_{SF}); 3) Survival fraction constant (K_{SF}) depending on the pharmaceutical substance and the target cell properties. It is noted that in the near future K_{SF} is expected to be routinely estimated based on the gene expression profile of the individual tumor under consideration, e.g., using DNA microarrays. More precisely the mean K_{SF} value based on population statistics will be perturbed based on the individual patient’s tumor gene expression profile. The survival fraction can be expressed as [58]

$$SF = e^{-K_{SF} \cdot T_{SF} \cdot C_{pav}}. \quad (2)$$

Use of O6-benzylguanine, an inhibitor of O6-methylguanine-DNA methyltransferase (MGMT) has been shown to eliminate MGMT in human glioma cell lines and increase their sensitivity to the clinically utilized alkylating agents BCNU (carmustine) and TMZ. This observation demonstrates that MGMT is an important mechanism of resistance to these alkylators and supports the use of O⁶-benzylguanine to reduce glioma resistance to alkylating agents. A graph of SF as a function of C_{pav} for the case of glioblastoma derived line UW455 has been used in order to calculate or better estimate the value of K_{SF} [43], [59], [60]. In the present model pre-treatment with O6-benzylguanine has been considered and therefore, the corresponding pharmacodynamics graph has been adopted [43], [59], [60]. K_{SF} has been calculated to be $9.2 \times 10^{-3} \mu\text{M}^{-1} \text{h}^{-1}$ when $SF = 10\%$ at $C_{pav} = 125 \mu\text{M}$. As a first approximation the parameter T_{SF} has been given the value of $t_{1/2} \approx 2 \text{ h}$ [38] which corresponds to the period of time during which the concentration of TMZ is above its half maximum value. The value $T_{SF} = t_{1/2} \approx 2 \text{ h}$ is given only to convey an idea of the time during which most of the effect of the drug takes place. The duration of the period for which the drug concentration is above its half maximum value is 1.7 h to 1.8 h (which if rounded to the nearest integer gives 2h) for each one of the first 5 days of the chemotherapeutic cycle [38]. The value of $T_{SF} = t_{1/2} \approx 2 \text{ h}$ if multiplied by the maximum concentration can be used as a first rough approximation of the area under the concentration *versus* time curve which appears at the exponent of (2). During the actual simulation process, the curve of drug concentration over time is discretized in intervals of 1 h. In each time interval the mean concentration of the drug

is calculated using the pharmacokinetics curve. The product of the mean drug concentration by 1h is used in the SF calculation equation for each one of the scanning intervals (of 1h each). Finally in this way the area under the concentration over time curve arises in the exponent of equation (2) as needed.

IV. THE MODEL BASICS

The notion of “geometrical cell” [18] is introduced in order to spatially describe the biological activity of the tumor [16], [17], [20]. A 3-D discretizing mesh is superimposed on the anatomical region of interest shown in the imaging data collected. Each geometrical cell of the mesh belonging to the tumor contains a number of biological cells “residing” in various phases within or out of the cell cycle (G1, S, G2, M, G0, Necrosis/Lysis, Apoptosis). Within each geometrical cell, a number of classes of biological cells (compartments), each one characterized by the phase in which its cells are found are defined. Sufficient registers are used in order to characterize the state of each geometrical cell and each phase class within it (e.g., the number of biological cells in phase G1, the time spent in phase G1, etc.). The number of biological cells constituting each phase class is initially estimated according to both the position of the geometrical cell within the tumor and the metabolic activity in the local area (e.g., based on PET, functional MRI, etc).

Mammalian cells require oxygen and nutrients for their survival and functional cells must, therefore, be located within a distance of 100 μm to 200 μm from the nearest capillary blood vessels, which is the diffusion limit for oxygen. For multicellular organisms to grow new blood vessels must be recruited by angiogenesis. Without blood vessels, tumors cannot grow beyond a critical size or metastasize to another organ [22]. In contrast to normal vessels, tumor vasculature is highly disorganized; vessels are tortuous and dilated, with uneven diameter, excessive branching and shunts. This is due to imbalance of angiogenic regulators. Consequently, tumor blood flow is chaotic and variable [22], [23] and leads to hypoxic and acidic regions in tumors [22], [23]. Tumor vessel ultrastructure is also abnormal. The vessel walls have numerous “openings” widened interendothelial junctions, and a discontinuous or absent basement membrane. These defects make tumor vessels “leaky” [25], [26] and there is tremendous heterogeneity in leakiness over space and time [20], [25], [26]. Vascular permeability and angiogenesis depend on the type of tumor and on the host organ in which the tumor is growing [22], [25].

Taking into account the previous observations, an intermediate layer between the “necrotic” and the “proliferating” layers of the tumor denoted by “G0” is assumed to exist. This layer which contains a substantial number of dormant cells lies around the necrotic area of the tumor. During the simulation process, and in the case of tumor growth, normal tissue capillaries are shifted away, and tumor capillaries are generated in their origin [22], [27]. Consequently, the new tumor cells are assumed to be sufficiently oxygenated and able to divide. The following temporal behavior assumptions are made: 1) Time is quantized and measured in appropriate units. In all applications described in this paper 1 h has been adopted as the unit of time. The discretizing mesh scanning procedure is described in detail in [18]. 2) Biological cells constituting each phase class within a given geometrical cell of the discretizing mesh are assumed to

be synchronized. 3) For each geometrical cell and for the pool of the chemotherapy affected cells, the time remaining until the next cell division is the result of weighting the time until the cell division of each synchronized cell subgroup of the pool by the number of cells constituting it. 4) For each geometrical cell under examination the remaining time in the current phase is reduced by one time unit (1 h) after each simulation step. 5) During the initialization process, cells within the same cell cycle phase class are not considered to be synchronized. A random number generator is used to produce a uniform cell distribution over the time units constituting the duration of each phase class within or out of the cell cycle. If the surviving cells of the entire tumor are reduced by three orders of magnitude (e.g., due to the effect of chemotherapy) a new random number generator is used in order to re-randomize the time elapsed within each phase for any given geometrical cell. This is done in order to avoid an artificial synchronization of the entire tumor. As at least the distribution of the cells in the various phases is respected, it has been shown that in this way no substantial error is introduced into the model's predictions. The tumor expansion and shrinkage algorithm adopted is described in [61]. The detailed mechanical behavior of the surrounding normal tissues as well as the local and whole body toxicities (e.g., epilepsy, neutropenia, thrombocytopenia, etc.) have not been taken into account in this version of the model. Especially toxicities need to be taken into account in detail (in a future model extension) as they impose fundamental restrictions on the prospective drug administration schedules. Furthermore, inclusion of the effects of drug resistance in more detail is expected to substantially refine the simulation model. The overall simulation strategy of the model presented is schematically depicted in Fig. 2. Table I provides a summary of the model parameters, some remarkable dependencies, their units, their values considered in this paper as well as the sources of the parameter values considered.

V. SIMULATION RUN AND VISUALIZATION

The computer code has been developed in Microsoft Visual C++ 6.0™. As far as computational demands are concerned execution of, e.g., a six week chemotherapy course (usually corresponding to 1.5 chemotherapy cycles) with a discretizing mesh of $96 \times 96 \times 96$ geometrical cells each one of dimensions $1 \text{ mm} \times 1 \text{ mm} \times 1 \text{ mm}$ on an AMD Athlon XP™ machine (2.5 GHz, 786 MB RAM) takes about 1.5 min. As the proposed model aims at serving as a decision support tool to a clinical doctor, *in silico* experiments should be performable in real-time. The imaging, histopathologic and eventual genetic data of the patient are processed by the previously described software in order to “predict” the most likely spatio-temporal response of the tumor. Software from Advanced Visual Systems™ has been used to provide a suite of sophisticated 3-D tools for presentation of the simulation results. Additionally, the simulation predictions have been visualized using the CAVE™ Immersive Virtual Reality System.

VI. THE CASE OF GRADE IV ASTROCYTOMA *IN VIVO*—RESULTS

A preliminary validation of the algorithms described so far has been achieved by devising and implementing the following testing procedure. A clinical case of glioblastoma multiforme

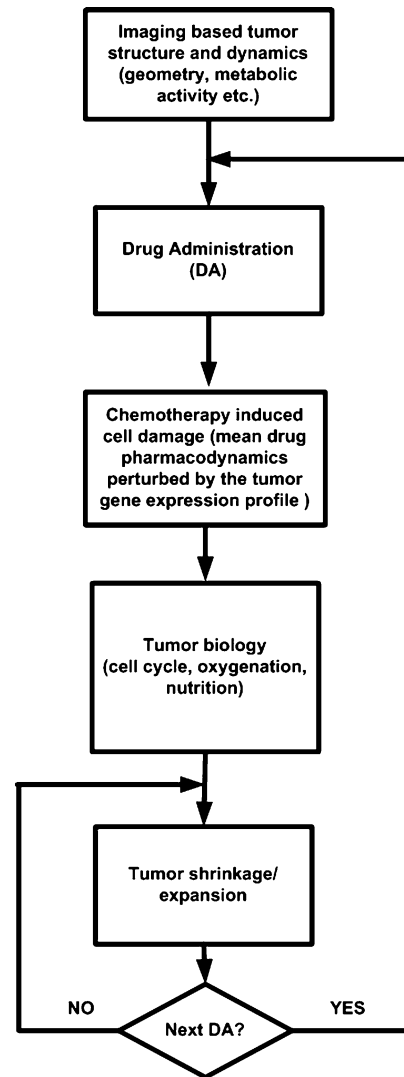


Fig. 2. A simplified flowchart of the proposed algorithm. Following introduction of the baseline tumor structure and metabolic activity data and the drug administration schedule, simulation of the various response stages takes place as shown in the flowchart.

(grade IV astrocytoma) has been selected and the imaging-based boundary of the tumor has been delineated. The necrotic area has also been identified, based on the corresponding T1 weighted, gadolinium enhanced MRI data. As a first approximation, the effective neovasculature field has been assumed to coincide with the area of the tumor where pronounced metabolism is apparent on the pertinent data. A discretizing mesh cube defining the anatomical region of interest has been superimposed on the imaging-based 3-D reconstruction of the anatomic region of interest. The dimensions of each geometrical cell of the cube are $1 \text{ mm} \times 1 \text{ mm} \times 1 \text{ mm}$. Such a volume contains roughly 10^6 biological cells [61],[62] ($\text{NBC} = 10^6$). The administered dose/chemotherapeutic fraction has been taken 150 mg/m^2 , or 200 mg/m^2 , or 250 mg/m^2 . The drug has been assumed to be administered orally, either once daily for 5 consecutive days/28-day treatment cycle (standard scheme, Fractionation scheme A, Fig. 3) or according to a hypothetical scheme in which drug administration is almost uniformly distributed throughout the chemotherapy cycle (Fractionation

TABLE I
SIMULATION MODEL PARAMETERS

	Parameter	Description	Some remarkable dependencies	Value	Unit	Reference
1		Patient's imaging data		e.g. T1 gadolinium enhanced MRI sections		
2	NBC	Number of biological cells included in one geometrical cell of the discretizing mesh		10^6	cells	[62]
3	CCD	"Mean" clonogenic cell density		10^7 , 2×10^4 , 3×10^4 , 4×10^4	cells / mm^3	[62] and perturbations
4	T_C	Cell cycle duration	Histopathology	30, 40, 48	h	[63], [65], [65]
5	T_{G1}	G1 phase duration	Histopathology	11 (Tc=30h), 15 (Tc=40h), 18 (Tc=48h)	h	[63], [65],[36], [63], [65],[36], [63], [65],[36]
6	T_S	S phase duration	Histopathology	13 (Tc=30h), 17 (Tc=40h), 21 (Tc=48h)	h	[63], [65],[36], [63], [65],[36], [63], [65],[36]
7	T_{G2}	G2 phase duration	Histopathology	4 (Tc=30h), 5 (Tc=40h), 6 (Tc=48h)	h	[63], [65],[36], [63], [65],[36], [63], [65],[36]
8	T_M	Mitosis duration	Histopathology	2 (Tc=30h), 3 (Tc=40h), 3 (Tc=48h)	h	[63], [65],[36], [63], [65],[36], [63], [65],[36]
9	T_{G0}	Maximum stay in the G0 phase before necrosis takes place		25	h	[63]
10	D	Dose per fraction (per m^2 of body surface)		150, 200, 250	mg/m^2	[38]
11		Time interval between fractions		See Fig. 3	h	[38] and perturbations
12	V_d	Volume of distribution (per Kg of body weight)		0.4	L (per kg of body weight)	[38]
13	k_a	Absorption rate constant		3.10 (for D=150 mg/m^2), 3.6 (for D=200 mg/m^2), 4.6 (for D=250 mg/m^2)	h^{-1}	calculated from [38]
14	k_{el}	Elimination rate constant		0.33 (for D=150 mg/m^2), 0.39 (for D=200 mg/m^2), 0.74 (for D=250 mg/m^2)	h^{-1}	calculated from [38]
15	$T_{SF} \approx t_{1/2}$	Duration of the interval where the drug concentration is above its half maximum value		2	h	[38]
16	K_{SF}	Survival fraction constant	Genetic/molecular profile	9.2×10^{-3}	$\mu\text{M}^{-1}\text{h}$	[43], [59], [60]
17		Cell loss factor		0.3		[18], [20]
18	W	Body weight of the patient		70	Kg	[36]

* It is noted that the values of the dose per fraction and the volume of distribution should be adjusted to the actual weight of the patient (e.g. 70 Kg).

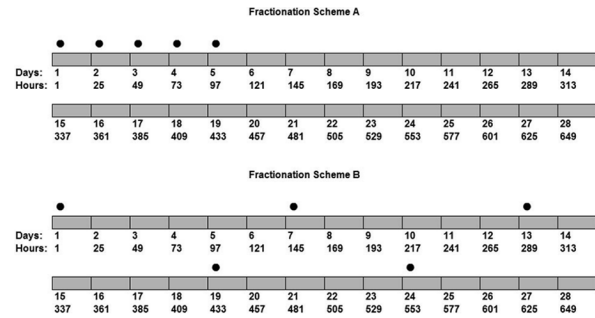


Fig. 3. The two chemotherapy fractionations considered. Fractionation A corresponds to the standard TMZ administration scheme (once daily for 5 consecutive days/28-day treatment cycle) whereas Fractionation B corresponds to a hypothetical drug administration almost uniformly distributed throughout the chemotherapy cycle. Each drug administration session is denoted by a small black disk (pill).

scheme B, Fig. 3). Only one chemotherapy cycle/scheme has been simulated.

For the specific type of poorly differentiated tumor under consideration, and for simplification reasons, all nonclonogenic cells have been considered to be necrotic (sterile cells have not been taken into account). The contribution of the living nonclonogenic cells (cells that are able to undergo only a limited number of cell divisions) are to be considered in a subsequent version of the model. A typical mean clonogenic cell density [62] is 10^7 cells/ cm^3 ($= 10^4$ cells/ mm^3). We have assumed a clonogenic cell density of 2×10^4 cells/ mm^3 in the "proliferating cell layer." This layer has lain between the external surface of the gross tumor volume and a hypothetical surface (HYP) enclosing its necrotic kernel and lying 1.5 mm further out. The tumor volume contained between HYP and the surface of the necrotic region has been assumed to contain a large number of dormant G0 cells; therefore, it is called "G0 cell layer". A clonogenic cell density of 10^4 cells/ mm^3 in the G0 cell layer and 0.2×10^4 cells/ mm^3 in the necrotic or dead cell layer of the tumor has also been assumed. Within each geometrical cell of the discretizing mesh the initial distribution of the clonogenic cells through the various cell cycle phases depends on the layer of the tumor to which the geometrical cell belongs. The following rough assumptions concerning the distribution of cells within and out of the cell cycle have been made. In the proliferating cell layer 70% of the living clonogenic cells have been assumed to be in the cycling phases and 30% in the G0 phase. In the G0 cell layer 30% of the living clonogenic cells have been assumed to be in the cycling phases and 70% in the G0 phase. Finally, in the necrotic cell layer 10% of the living clonogenic cells have been assumed to be in the cycling phases and 90% in the G0 phase. The previous fractions reflect an initial effort to quantify histopathological observations concerning the cytokinetic distribution of the tumor cells in the various layers of a tumor. More realistic values are expected to arise during the clinical validation of the model.

Further parameters of importance include the cell cycle duration (T_C) assumed to be 30 h and the cell cycle phase durations (T_{G1} , T_S , T_{G2} , T_M , and T_{G0}) assumed to be 11 h, 13 h, 4 h, 2 h, and 25 h, respectively [63]. The *free tumor growth* cell loss factor [18] has been taken to be 0.3 as cell death products are removed from brain with considerable difficulty. This total cell

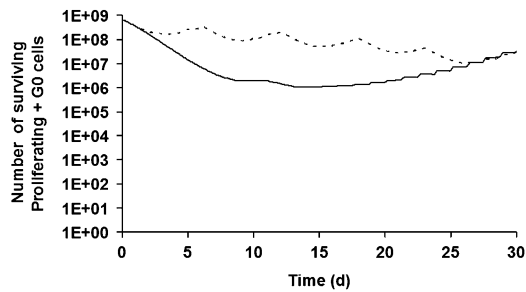


Fig. 4. Number of surviving (metabolically living) proliferating and dormant (G0) tumor cells corresponding to the particular GBM tumor considered as a function of the time. TMZ is administered according to fractionation scheme A (solid line) or B (dashed line) (Fig. 3). Each chemotherapy fraction corresponds to 150 mg/m^2 . The cell cycle has been assumed equal to $T_c = 30 \text{ h}$ and the mean clonogenic cell density equal to $\text{CCD} = 10^4 \text{ cells/mm}^3$ (clonogenic cell density in the *proliferating cell layer* = $2 \times 10^4 \text{ cells/mm}^3$). Only one chemotherapy cycle/scheme has been simulated.

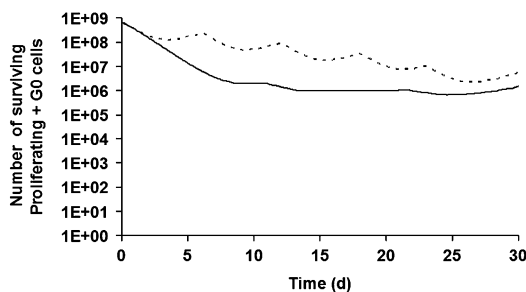


Fig. 5. Number of surviving (metabolically living) proliferating and dormant (G0) tumor cells corresponding to the particular GBM tumor considered as a function of the time. TMZ is administered according to fractionation scheme A (solid line) or B (dashed line) (Fig. 3). Each chemotherapy fraction corresponds to 200 mg/m^2 . The cell cycle has been assumed equal to $T_c = 30 \text{ h}$ and the mean clonogenic cell density equal to $\text{CCD} = 10^4 \text{ cells/mm}^3$ (clonogenic cell density in the *proliferating cell layer* = $2 \times 10^4 \text{ cells/mm}^3$). Only one chemotherapy cycle/scheme has been simulated.

loss factor has been expressed as the sum of the cell loss factor due to necrosis (assumed to be 0.2) and the cell loss factor due to apoptosis (assumed to be 0.1). It is noted that necrosis tends to be more pronounced than apoptosis for the specific type of tumor. The probabilities of cell loss/hour due to necrosis and due to apoptosis have been derived from the above-mentioned value of the cell loss factor according to Steel [20]. More realistic values of the cell loss factor and the phase distribution of cells in the various tumor layers are expected to emerge after completion of the clinical adaptation process.

As already mentioned, in order to assess the model's sensitivity to various critical input parameters, the following parametric analysis has been performed. Three different doses/fraction have been considered: 150 mg/m^2 , 200 mg/m^2 and 250 mg/m^2 . Both the standard fractionation scheme A and the hypothetical fractionation scheme B (Fig. 3) have been considered for each dose/fraction. The only scheme performance criterion adopted so far is tumor control. Figs. 4–6 show the number of surviving proliferating and G0 cells. It should be stressed that Figs. 4–6 refer to the total number of (still) metabolically active cells. This implies that surviving proliferating and G0 cells include also cells affected by the drug and destined to die but not yet dead. The reason for considering this set of cells is that metabolically active cells exploit the sufficient blood provision

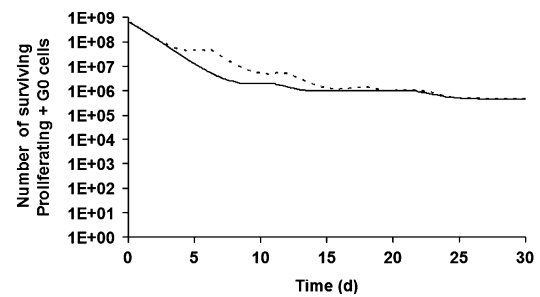


Fig. 6. Number of surviving (metabolically alive) proliferating and dormant (G0) tumor cells corresponding to the particular GBM tumor considered as a function of the time. TMZ is administered according to fractionation scheme A (solid line) or B (dashed line) (Fig. 3). Each chemotherapy fraction corresponds to 250 mg/m^2 . The cell cycle has been assumed equal to $T_c = 30 \text{ h}$ and the mean clonogenic cell density equal to $\text{CCD} = 10^4 \text{ cells/mm}^3$ (clonogenic cell density in the *proliferating cell layer* = $2 \times 10^4 \text{ cells/mm}^3$). Only one chemotherapy cycle/scheme has been simulated.

which creates the hyperintense regions on the T1 contrast enhanced MRI or PET slices. According to Fig. 4, in the case of a fraction dose of 150 mg/m^2 , the standard fractionation scheme A seems to be superior to the hypothetical scheme B, as it keeps the number of surviving cells substantially lower during most of the chemotherapy 28 d cycle. This implies that eventual combination of TMZ chemotherapy with another cytotoxic modality (e.g., irradiation) might lead to a considerably improved outcome. Two fighting strategies can be distinguished here. The first one aims at keeping cell survival low by an initial fast suppression of tumor repopulation whereas the second one aims at reducing cell survival by delivering cytotoxicity more uniformly in time. The adoption of the first strategy in the clinical setting is in accordance with the simulation predictions. According to Fig. 5 the standard fractionation scheme A leads to a better tumor control outcome than the more uniform fractionation scheme B and this happens during the entire duration of the cycle. This prediction is also in agreement with clinical practice. Even in the case of a 250 mg/m^2 dose/fraction a superiority of fractionation scheme A to B is clear according to Fig. 6. Therefore, although still from a rather qualitative point of view, the simulation model seems to be able to reasonably respond to changes in critical parameters and at the same time to support selection of particular fractionation schemes.

The theoretical predictions shown in Fig. 7 visualize the ability of the model to effectively simulate the tumoricidal effect of Temozolomide. As TMZ is a CCNS agent it is expected to kill the majority of both the dormant (G0) and the proliferating cells. This remark is compatible with Fig. 7(b)–(d). Details on the simulation sequences and the visualization criteria are given on the corresponding figure captions. Repopulation between chemotherapy cycles, a usually neglected but crucial factor which affects the overall treatment output [64], is clearly visualized in Figs. 4–6.

In order to extend the study of the model behavior to other combinations of possible values of the model parameters, a number of further simulation runs have been performed. Figs. 8–10 depict the simulation predictions concerning the two fractionation schemes considered for other possible values of the cell cycle duration and clonogenic cell density. In particular Fig. 8 corresponds to $T_c = 48 \text{ h}$, mean clonogenic cell

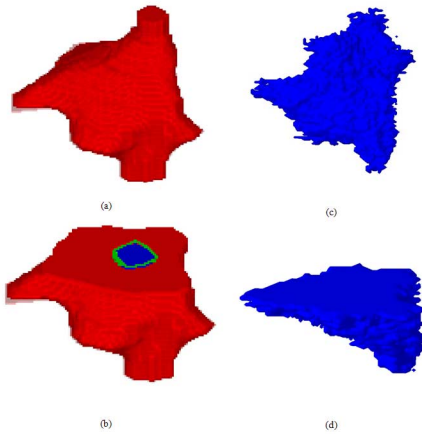


Fig. 7. Three-dimensional visualization of the simulated response of a clinical glioblastoma multiforme tumor to one cycle of chemotherapeutic scheme (150 mg/m² orally once daily for 5 consecutive days/28-day treatment cycle, [fractionation scheme A]). (a) External surface of the tumor before the beginning of chemotherapy, (b) internal structure of the tumor before the beginning of chemotherapy, (c) external surface of the tumor 20 days after the beginning of chemotherapy, and (d) internal structure of the tumor 20 days after the beginning of chemotherapy. Pseudocolor Code: dark grey: proliferating cell layer, light grey: dormant cell layer (G0), black: dead cell layer. The following “99.8%” criterion has been devised and applied: “For a geometrical cell of the discretizing mesh, if the percentage of dead cells within it is lower than 99.8% then [if percentage of proliferating cells > percentage of G0 cells, then paint the geometrical cell dark grey (proliferating cell layer), else paint the geometrical cell light grey (G0 cell layer)] else paint the geometrical cell black (dead cell layer)”. Three-dimensional visualization of the simulated response of a clinical glioblastoma multiforme tumor to one cycle of chemotherapeutic scheme [150 mg/m² orally once daily for 5 consecutive days/28-day treatment cycle, (fractionation scheme A)]. (a) External surface of the tumor before the beginning of chemotherapy, (b) internal structure of the tumor before the beginning of chemotherapy, (c) external surface of the tumor 20 days after the beginning of chemotherapy, and (d) internal structure of the tumor 20 days after the beginning of chemotherapy. Pseudocolor Code: red: proliferating cell layer, green: dormant cell layer (G0), blue: dead cell layer. The following “99.8%” criterion has been devised and applied: “For a geometrical cell of the discretizing mesh, if the percentage of dead cells within it is lower than 99.8% then [if percentage of proliferating cells > percentage of G0 cells, then paint the geometrical cell red (proliferating cell layer), else paint the geometrical cell green (G0 cell layer)] else paint the geometrical cell blue (dead cell layer)”. (Color version available online at <http://ieeexplore.ieee.org>.)

density equal to 2×10^4 cells/mm³ and dose/fraction equal to 150 mg/m². Fig. 9 corresponds to $T_C = 40$ h, mean clonogenic cell density equal to 3×10^4 cells/mm³ and dose/fraction equal to 200 mg/m². Fig. 10 corresponds to $T_C = 40$ h, mean clonogenic cell density equal to 4×10^4 cells/mm³ and dose/fraction equal to 200 mg/m². It is noted that the values of 48 h and 40 h have been randomly selected from the range 1–2.5 days of possible T_C values for gliomas as estimated by Pertuiset *et al.* [65].

It is pointed out that due to the complex interdependence of the parameters involved in advanced (and detailed) tumor simulation models, no monotonicity between the model prediction outcome and the parameters involved can be strictly assumed. Theoretically, one should perform an infinite number of simulations corresponding to all possible values of the parameters involved. However, as this would be unrealistic, the best practical approach is to select a representative finite number of highly possible parameter values and study the tumor phenomenon through this simplified window. Obviously, such an approach

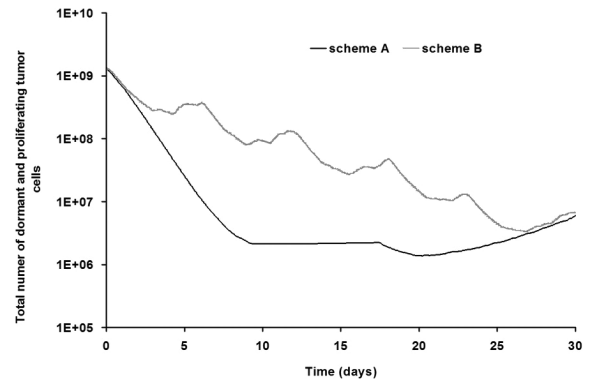


Fig. 8. Number of surviving (metabolically living) proliferating and dormant (G0) tumor cells corresponding to the particular GBM tumor considered as a function of the time. TMZ is administered according to fractionation scheme A (bold line) or B (light line) (Fig. 3). Each chemotherapy fraction corresponds to 150 mg/m². The cell cycle has been assumed equal to $T_c = 48$ h and the mean clonogenic cell density equal to $2 \times CCD = 2 \times 10^4$ cells/mm³ (clonogenic cell density in the *proliferating cell layer* = 4×10^4 cells/mm³). Only one chemotherapy cycle/scheme has been simulated.

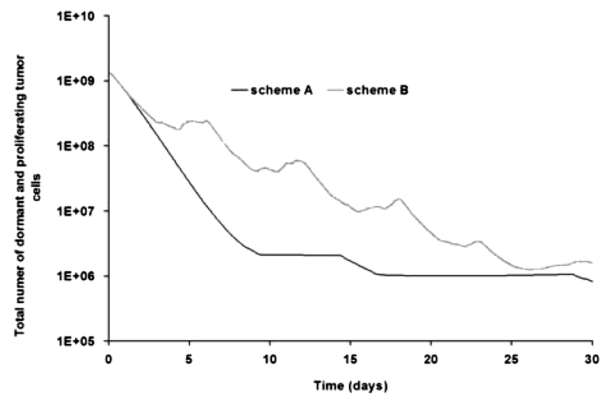


Fig. 9. Number of surviving (metabolically living) proliferating and dormant (G0) tumor cells corresponding to the particular GBM tumor considered as a function of the time. TMZ is administered according to fractionation scheme A (bold line) or B (light line) (Fig. 3). Each chemotherapy fraction corresponds to 200 mg/m². The cell cycle has been assumed equal to $T_c = 40$ h and the mean clonogenic cell density equal to $3 \times CCD = 3 \times 10^4$ cells/mm³ (clonogenic cell density in the *proliferating cell layer* = 6×10^4 cells/mm³). Only one chemotherapy cycle/scheme has been simulated.

(as adopted in this paper) is directly dictated by the hyper-complex nature of cancer itself and it seems that there is no way to evade it. Nevertheless, as high computer power is increasingly available, large statistical “ensembles” of computer simulations are expected to be routinely performed.

VII. DISCUSSION

All simulation predictions presented in the forms of graphs and multidimensional visualizations agree at least qualitatively with clinical experience. A process of quantitative clinical adaptation and validation of the evolving model is ongoing in collaboration with several clinical centers. Such a validation procedure involves comparison of the model predictions with pertinent clinical data before, during, and after a number of chemotherapeutic cycles. The simulation model can just “follow” the clinical practice and activate a self-optimization procedure. This implies that in case that substantial divergence between the simulations predictions and the actual clinical

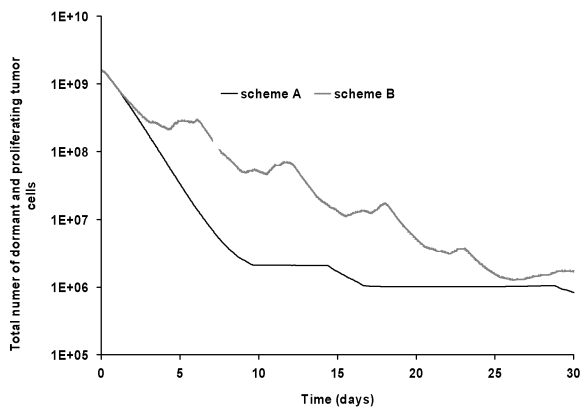


Fig. 10. Number of surviving (metabolically living) proliferating and dormant (G0) tumor cells corresponding to the particular GBM tumor considered as a function of the time. TMZ is administered according to fractionation scheme A (bold line) or B (light line) (Fig. 3). Each chemotherapy fraction corresponds to 200 mg/m^2 . The cell cycle has been assumed equal to $T_c = 40 \text{ h}$ and the mean clonogenic cell density equal to $4 \times \text{CCD} = 4 \times 10^4 \text{ cells/mm}^3$ (clonogenic cell density in the *proliferating cell layer* = $8 \times 10^4 \text{ cells/mm}^3$). Only one chemotherapy cycle/scheme has been simulated.

outcomes is observed, perturbations of the model parameter values in combination with the use of pertinent optimization techniques such as artificial neural networks, genetic algorithms, etc. are activated. Thus, better adapted parameter values are expected to emerge. *Self optimization* does not necessarily require clinical trials specifically designed for the validation of the model. Data stemming from the current clinical practice can be used in order to considerably optimize the model. Hence, no major ethical concerns are expected to arise during the clinical validation-adaptation procedure. The fact that the simulation model has a clear modular character is expected to substantially facilitate its clinical adjustment and application. Simulation of the reaction of normal tissues to TMZ chemotherapy is under development. Ongoing integration of DNA microarray output in conjunction with molecular data interpreting gene-protein-drug networks are expected to strengthen the model's predictive potential. Furthermore, an adaption of the model so that the concurrent behavior of several grades of malignancy is taken into account would be another clinically important extension.

Our research group has already developed a novel 4-D model of the response of *in vivo* tumors to fractionated radiation therapy [18], [61], [66] which is envisaged to be merged with the proposed chemotherapy model at a later stage. Due to the high complexity of the combined problem, there is no alternative to a multistep procedure. A refinement of both models should take place before their envisaged merging. Besides, temozolomide may be prescribed as monotherapy to recurrent gliomas. It should also be mentioned that provided that the beginning of a chemotherapy cycle and the end of a preceding radiotherapy course are quite distant, the effect of irradiation *exclusively* on the imageable tumor is expected to have been included in the "necrosed" areas of the tumor identifiable through imaging techniques.

It is pointed out that although a quantitatively refined model would take some time to complete, the simulation model proposed can be used as a tool to perform extensive exploratory parametric studies in the meantime. This implies that the model can be used in order to identify those parameters that play the

most crucial role in the prediction outcome of the simulation and consequently in the prediction of the natural phenomenon itself. Such identifications are expected to lead to suggestions for targeted experimental work in order to refine the estimates of the most critical parameters. At the same time new questions stimulating well targeted experimental, theoretical and clinical research are expected to emerge.

VIII. CONCLUSION

The 4-D, patient individualized *in vivo* simulation model of tumor response to temozolomide-based chemotherapy presented in this paper constitutes a novel approach towards the biological optimization of cancer treatment. An at least qualitative agreement of the model's predictions with clinical experience strengthens its treatment optimization potential. Systematic long term clinical testing that is currently under way is expected to lead to both its algorithmic refinement and better parameter value selection. After completion of the clinical adaptation and validation procedure of the proposed model, an integrated, patient individualized decision support and temporal treatment planning system is expected to emerge. Significantly, it could serve as an educational platform for professionals and patients by means of virtual reality demonstrations of the likely natural development and treatment responsiveness of specific cancers so that all groups might positively contribute to the discussion about treatment procedure.

ACKNOWLEDGMENT

The authors would like to thank Dr. D. Dionysiou, National Technical University of Athens, for her support on the imaging part of this work (development of the segmentation tool).

REFERENCES

- [1] S. Chuang, "Mathematic models for cancer chemotherapy: pharmacokinetic and cell kinetic considerations," *Cancer Chemother. Rep.*, vol. 59, no. 4, pp. 827–42, 1975.
- [2] V. A. Levin, C. S. Patlak, and H. D. Landahl, "Heuristic modeling of drug delivery to malignant brain tumors," *J. Pharmacokinet. Biopharm.*, pp. 257–2968, 1980.
- [3] S. Ozawa, Y. Sugiyama, J. Mitsuhashi, and M. Inaba, "Kinetic analysis of cell killing effect induced by cytosine arabinoside and cisplatin in relation to cell cycle phase specificity in human colon cancer and chinese hamster cells," *Cancer Res.*, vol. 49, pp. 3823–3828, 1989.
- [4] Y. Jean, J. De Traversay, and P. Lemieux, "Teaching cancer chemotherapy by means of a computer simulation," *Int. J. Biomed. Comput.*, vol. 36, pp. 273–280, 1994.
- [5] F. K. Nani and M. N. Oguztereli, "Modelling and simulation of chemotherapy of haematological and gynaecological cancers," *IMA J. Math. Appl. Med. Biol.*, vol. 16, pp. 39–91, 1999.
- [6] A. Iliadis and D. Barbolosi, "Optimizing drug resistance in cancer chemotherapy by an efficacy-toxicity mathematical model," *Comput. Biomed. Res.*, vol. 33, pp. 211–226, 2000.
- [7] D. Barbolosi and A. Iliadis, "Optimizing drug regimens in cancer chemotherapy: A simulation study using a PK-PD model," *Comput. Biol. Med.*, vol. 31, pp. 157–172, 2001.
- [8] J. Davis and I. F. Tannock, "Repopulation of tumour cells between cycles of chemotherapy: A neglected factor," *The Lancet Oncol.*, vol. 1, pp. 86–93, 2000.
- [9] S. N. Gardner, "Modeling multi-drug chemotherapy: Tailoring treatment to individuals," *J. Theor. Biol.*, vol. 214, pp. 181–207, 2002.
- [10] J. P. Ward and J. R. King, "Mathematical modeling of drug transport in tumour multicell spheroids and monolayer cultures," *Mater. Biosci.*, vol. 181, pp. 177–207, 2003.
- [11] S.M. Haney, P.M. Thompson, T.F. Cloughesy, J.R. Alger, and A.W. Toga, "Tracking tumor growth rates in patients with malignant gliomas: A test of two algorithm," *Amr J. Neuroradiol.*, vol. 22, no. 1, pp. 73–82, 2001.

- [12] M. Prastawa, E. Bullitt, N. Moon, K. Leemput, and G. Gerig, "Automatic brain segmentation by subject specific modification of atlas priors," *Acad. Radiol.*, vol. 10, no. 12, pp. 1341–8, 2003.
- [13] A. Kansal, S. Torquato, G. Harsh, E. Chiocca, and T. Deisboeck, "Simulated brain tumor growth dynamics using a three-dimensional cellular automaton," *J. Theor. Biol.*, vol. 203, pp. 367–382, 2000.
- [14] K. R. Swanson, C. Bridge, J. D. Murray, and E. C. Alvord, Jr., "Virtual and real brain tumors: Using mathematical modeling to quantify glioma growth and invasion," *J. Neurol. Sci.*, vol. 216, pp. 1–10, 2003.
- [15] K. Swanson, E. C. Alvord, Jr., and J. D. Murray, "Dynamics of a model for brain tumors reveals a small window for the therapeutic intervention," *Discrete Continuous Dynamical Syst.-Ser. B*, vol. 4, no. 1, pp. 289–295, 2004.
- [16] Lodish D. Baltimore, A. Berk, S. Zipursky, P. Matsudaira, and J. Darnell, *Molecular Cell Biology*. New York: Scientific American Books, 1995, pp. 1247–1294.
- [17] Perez and L. Brady, Eds., *Principles and Practice of Radiation Oncology*. Philadelphia, PA: Lippincott-Raven, 1998.
- [18] S. Stamatakos, D. D. Dionysiou, E. I. Zacharaki, N. A. Mouravliansky, K. S. Nikita, and N. K. Uzunoglu, "In silico radiation oncology: Combining novel simulation algorithms with current visualization techniques," *Proc. IEEE*, vol. 90, no. 1, pp. 1764–1777, 2002.
- [19] W. Duechting, T. Ginsberg, and W. Ulmer, "Modeling of radiogenic responses induced by fractionated irradiation in malignant and normal tissue," *Stem Cells*, vol. 13, no. 1, pp. 301–306, 1995.
- [20] G. Steel, Ed., *Basic Clinical Radiobiology*, 3rd ed. London, U.K.: Arnold, 2002, pp. 165–168, pp. 13, 52–63.
- [21] B. Ribba, K. Marron, Z. Agur, T. Alarcon, and P. K. Maini, "A mathematical model of doxorubicin treatment efficacy for non-Hodgkin's lymphoma: Investigation of the current protocol through theoretical modeling results," *Bull. Math. Biol.*, vol. 67, pp. 79–99, 2005.
- [22] P. Carmeliet and R. K. Jain, "Angiogenesis in cancer and other diseases," *Nature*, vol. 407, pp. 249–259, 2002.
- [23] W. Baish and R. F. Jain, "Fractals and cancer," *Cancer Res.*, vol. 60, pp. 3683–3688, 2000.
- [24] G. Helmlinger, F. Yuan, M. Dellian, and R. K. Jain, "Interstitial pH and pO₂ gradients in solid tumors in vivo: High-resolution measurements reveal a lack of correlation," *Nature Med.*, vol. 3, pp. 177–182, 1997.
- [25] S. K. Hobbs, W. L. Monsky, F. Yuan, W. G. Roberts, L. Griffith, V. P. Torchilin, and R. K. Jain, "Regulation of transport pathways in tumor vessels: Role of tumor type and microenvironment," *Proc. Nat. Acad. Sci., USA*, vol. 95, pp. 4607–4612, 1998.
- [26] H. Hashizume, P. Baluk, S. Morikawa, J. W. McLean, G. Thurston, S. Roberge, R. K. Jain, and D. M. McDonald, "Openings between defective endothelial cells explain tumor vessel leakiness," *Am. J. Pathol.*, vol. 156, pp. 1363–1380, 2000.
- [27] Michelson and J. T. Leith, "Positive feedback and angiogenesis in tumor growth control," *Bull. Math. Biol.*, vol. 59, no. 2, pp. 233–254, 1997.
- [28] S. Agarwala and J. Kirkwood, "Temozolomide, a novel alkylating agent with activity in the central nervous system, may improve the treatment of advanced metastatic melanoma," *The Oncologist*, vol. 5, pp. 144–151, 2000.
- [29] E. S. Newlands, M. F. Stevens, S. R. Wedge, R. T. Wheelhouse, and C. Brock, "Temozolomide: A review of its discovery, chemical properties, pre-clinical development and clinical trials," *Cancer Treat. Rev.*, vol. 23, pp. 35–61, 1997.
- [30] M. J. M. Darks, G. L. Plosker, B. Jarvis, and Temozolomide, "A review of its use in the treatment of malignant gliomas, malignant melanoma and other advanced cancers," *Am. J. Cancer*, vol. 1, no. 1, pp. 55–80, 2002.
- [31] Watson, N. Hopkins, J. Roberts, J. Steitz, and A. Weiner, *Molecular Biology of the Gene*, 4th ed. Menlo Park, CA: Benjamin/Cummings, 1987, pp. 1006–1096.
- [32] G. Stamatakos, D. Dionysiou, N. Mouravliansky, K. Nikita, G. Pissakos, P. Georgolopoulou, and N. Uzunoglu, "Algorithmic description of the biological activity of a solid tumor in vivo," in *Proc. EUROSIM 2001 Congress*, Delft, The Netherlands, Jun. 26–29, 2001, (CD-ROM).
- [33] G. Stamatakos, E. I. Zacharaki, N. K. Uzunoglu, and K. S. Nikita, "Tumor growth and response to irradiation in vitro: A technologically advanced simulation model," in *Int. J. Radiat. Oncol. Biol. Phys.*, 2001, vol. 51, no. 1, pp. 240–241.
- [34] J. F. Jen, D. L. Cutler, S. M. Pai, V. K. Batra, M. B. Affrime, D. N. Zambas, S. Heft, and G. Hajian, "Population pharmacokinetics of temozolomide in cancer patients," *Pharm. Res.*, vol. 17, no. 9, pp. 1284–1289, 2000.
- [35] R. C. Bast, D. W. Kufe, R. E. Pollock, R. R. Weichselbaum, J. F. Holland, and E. Frei, *Holland-Frei Cancer Medicine*, 6th ed. Hamilton, ON, Canada: BC Decker, 2000.
- [36] B. G. Katzung, *Basic and Clinical Pharmacology*, 8th ed. New York: McGraw-Hill/Lange Medical Books, 2001.
- [37] M. C. Perry, Ed., *The Chemotherapy Source Book*, 3rd ed. Philadelphia, PA: Lippincott Williams and Wilkins, 2001.
- [38] "FDA, Center for Drug Evaluation and Research," Drug Name: Temozolomide (Temodal), New Drug Application, Clinical Pharmacology and Biopharmaceutics Reviews pp. 19–20, Revision date: 2/2/1999, Application Number: 21029.
- [39] Temodal (Temozolomide) Capsules-Product Information NJ, 1999, FDA, Department of Center for Drug Evaluation and Research.
- [40] J. Ma, M. Murphy, P. J. O'Dwyer, E. Berman, K. Reed, and J. M. Gallo, "Biochemical changes associated with a multidrug-resistant phenotype of a human glioma cell line with temozolomide-acquired resistance," *Biochem. Pharmacol.*, vol. 63, pp. 1219–1228, 2002.
- [41] S. S. Agarwala and J. M. Kirkwood, "Temozolomide in combination with interferon alpha-2b in patients with metastatic melanoma: A phase I dose-escalation study," *Cancer*, vol. 97, pp. 121–127, 2003.
- [42] W. Günther, E. Pawlak, R. Damasceno, H. Arnold, and A. J. Terzis, "Temozolomide induces apoptosis and senescence in glioma cells cultured as multicellular spheroids," *Br. J. Cancer.*, vol. 88, pp. 463–469, 2003.
- [43] J. R. Silber, M. S. Bobola, T. G. Ewers, M. Muramoto, and M. S. Berger, "O⁶-alkylguanine DNA-alkyltransferase is not a major determinant of sensitivity to 1,3-bis(2-chloroethyl)-1-nitrosourea in four medulloblastoma cell lines," *Oncol. Res.*, vol. 4, pp. 241–248, 1992.
- [44] M. Brada, "A phase I study of SCH52365 (Temozolomide) in adult patients with advanced cancer," in *Proc. Am. Soc. Clinical Oncology*, 1995, vol. 14, no. 470.
- [45] E. S. Newlands, "Phase I Trial of Temozolomide (CCRG 81045: M&B 39831: NSC 362856)," *Br. J. Cancer*, vol. 65, pp. 287–291, 1992.
- [46] R. Stupp, "Promising survival with concomitant and adjuvant temozolomide for newly diagnosed glioblastoma multiforme," in *Proc. A. Soc. Clin. Oncol.*, New Orleans, LA, May 2000, 19, Abstract (632), 20–23, ASCO, 36th Ann. Mtg..
- [47] R. Stupp, M. Gander, S. Leyvraz, and E. Newlands, "Current and future developments in the use of temozolomide for the treatment of brain tumours," *Lancet Oncol. Rev.*, vol. 2, no. 9, pp. 552–560, 2001.
- [48] M. Mayersohn and M. Gibaldi, "Mathematical Methods in Pharmacokinetics. I Use of the Laplace Transform for Solving Differential Rate Equations," *Am. J. Pharm., Education*, vol. 34, pp. 608–614, 1970.
- [49] M. Mayersohn and M. Gibaldi, Amer. J. Pharm., Ed., "Mathematical Methods in Pharmacokinetics II Solution of the Two Compartment Open Model," *Am. J. Pharm. Educ.*, vol. 35, pp. 19–28, 1971.
- [50] L. Z. Benet, "General treatment of linear mammillary models with elimination from any compartment as used in pharmacokinetics," *J. Pharm. Sci.*, vol. 61, pp. 536–541, 1972.
- [51] O. L. Chinot, S. Honore, H. Dufour, M. Barrie, D. Figarella-Branger, X. Muracciole, D. Braguer, P. M. Martin, and F. Grisoli, "Safety and efficacy of temozolomide in patients with recurrent anaplastic oligodendrogliomas after standard radiotherapy and chemotherapy," *J. Clin. Oncol.*, vol. 19, no. 2, pp. 449–55, 2001.
- [52] J. G. Douglas and K. Margolin, "The treatment of brain metastases from malignant melanoma," *Semin. Oncol.*, vol. 29, pp. 518–524, 2002.
- [53] B. L. Ebert, E. Niemierko, K. Shaffer, and R. Salgia, "Use of temozolomide with other cytotoxic chemotherapy in the treatment of patients with recurrent brain metastases from lung cancer," *Oncologist*, vol. 8, pp. 69–75, 2003.
- [54] D. C. Crafts, T. Hoshino T, and Wilson CB, "Current status of population kinetics in gliomas," *Bull. Cancer*, vol. 64, pp. 115–124, 1977.
- [55] D. D. Shoemaker, P. J. O'Dwyer, S. Marsoni, J. Plowman, J. P. Davignon, and R. D. Davis, "Spiromustine: A new agent entering clinical trials," *Invest New Drugs*, vol. 1, pp. 303–308, 1983.
- [56] W. J. Jusko, "Pharmacodynamics of chemotherapeutic effects: Dose-time-response relationships for phase-nonspecific agents," *J. Pharm. Sci.*, vol. 60, no. 6, pp. 892–895, 1971.
- [57] H. E. Skipper, F. M. Schabel, L. B. Mellett, J. A. Montgomery, L. J. Wilkoff, H. H. Lloyd, and R. W. Brockman, "Implications of biochemical, cytokinetic, pharmacologic, and toxicologic relationships in the design of optimal therapeutic schedules," *Cancer Chemother.*, vol. 54, pp. 431–450, 1970.
- [58] H. Eichholtz-Wirth, "Dependence of the cytostatic effect of adriamycin on drug concentration and exposure time in vitro," *Br. J. Cancer*, vol. 41, pp. 886–891, 1980.
- [59] M. S. Bobola, S. H. Tseng, A. Blank, M. S. Berger, and J. R. Silber, "Role of O⁶-methylguanine-DNA methyltransferase in resistance of human brain tumor cell lines to the clinically relevant methylating agents temozolomide and streptozotocin," *Clin. Cancer Res.*, vol. 2, pp. 735–741, 1996.

- [60] M. S. Bobola, M. S. Berger, and J. R. Silber, "Contribution of O6-methylguanine-DNA methyltransferase to resistance to 1,3-(2-chloroethyl)-1-nitrosourea in human brain tumor-derived cell lines," *Mol. Carcinog.*, vol. 13, pp. 81–88, 1995.
- [61] V. Antipas, G. S. Stamatakos, N. Uzunoglu, D. Dionysiou, and R. Dale, "A spatiotemporal simulation model of the response of solid tumors to radiotherapy *in vivo*: Parametric validation concerning oxygen enhancement ratio and cell cycle duration," *Phys. Med. Biol.*, vol. 49, pp. 1–20, 2004.
- [62] Nahum and B. Sanchez-Nieto, "Tumor control probability modelling: Basic principles and applications in treatment planning," *Physica Medica*, vol. 17, no. 2, pp. 13–23, 2001.
- [63] W. Duechting, W. Ulmer, R. Lehrig, T. Ginsberg, and E. Dedeleit, "Computer simulation and modeling of tumor spheroid growth and their relevance for optimization of fractionated radiotherapy," *Strahlenther. Onkol.*, vol. 168, no. 6, pp. 354–360, 1992.
- [64] A. J. Davis and I. F. Tannock, "Repopulation of tumour cells between cycles of chemotherapy: A neglected factor," *Lancet Oncol.*, vol. 1, pp. 86–93, 2000.
- [65] B. Pertuiset B, D. Dougherty, C. Cromeyer, T. Hoshino, M. Berger, and M.L.J. Rosenblum, "Stem cell studies of human malignant brain tumours Part 2: Proliferation kinetics of brain-tumour cells *in vitro* in early-passage cultures," *Neurosurgery*, vol. 63, no. 3, pp. 426–32, 1985.
- [66] D.D. Dionysiou, G.S. Stamatakos, N.K. Uzunoglu, K.S. Nikita, and A. Marioli, "A Four dimensional *in vivo* model of tumour response to radiotherapy: Parametric validation considering radiosensitivity, genetic profile and fractionation," *J. Theor. Biol.*, vol. 230, pp. 1–20, 2004.



Georgios S. Stamatakos was born at Amyclae, Sparta, Greece, in 1963. He received the Diploma degree in electrical engineering from the National Technical University of Athens, Athens (NTUA), Greece, in 1987, the M.Sc. degree in bioengineering from the University of Strathclyde, Glasgow, U.K., in 1988, and the Ph.D. degree in physics (biophysics) from NTUA in 1997.

In 1999 he completed a postdoctoral fellowship research project on medical technology in NTUA. From 1989 to 1990, he was with the Hellenic Army General Staff, Medical Corps Directorate. Between 1991 and 1997, he was employed as Teaching Assistant in the Physics Department, NTUA. Since 1997, he has been a Researcher at the Institute of Communication and Computer Systems (ICCS), Department of Electrical and Computer Engineering, NTUA, where he is currently a Research Associate Professor in the field of "Analysis and Simulation of Biological Systems and their Interaction with Electromagnetic Radiation." He is the Scientific Coordinator of the *In Silico* Oncology Group, NTUA, and a teaching staff member of the Postgraduate School of Electronics Officers (STIAD), Athens. His research interests include oncological simulations (*in silico* oncology), radiotherapy, and chemotherapy optimization, bioinformatics, electromagnetic propagation and scattering, bioelectromagnetics, radiation safety, and biooptics. He has published over 60 papers in international journals, conference proceedings, and books. He has been involved as researcher/team leader in several European Commission research and development projects such as EUROMED/DGIII, CEPHOS/SMT, ACGT/IST, etc. He is an Associate Editor of *Cancer Informatics*.

Dr. Stamatakos is a member of the Technical Chamber of Greece, the European Society for Engineering and Medicine, the American Association for the Advancement of Science, and the Center for the Development of a Virtual Tumor supported by the US NIH-National Cancer Institute through the Integrative Cancer Biology Program (CA113004).



Vassilis P. Antipas (S'02) was born in Athens, Greece, in 1977. He received the Bachelor degree in electrical and electronic engineering from the School of Engineering, University of Sussex, Sussex, U.K., in 1999, and the Diploma and M.Sc. degrees in engineering and physical science in medicine, from the Department of Biological and Medical Systems, Imperial College of Science, Technology and Medicine and the University of London, London, U.K., in 2000. He is currently working towards the Ph.D. degree in the Department of Electrical and Computer Engineering, the National Technical University of Athens (NTUA).

During 1998 he was with "CLIPSAL HELLAS" and the Advanced Research and Therapeutic Institute of Athens "O ENCEPHALOS" S.A. His research interests include oncological simulations and modeling, biological process simulation, systems analysis and biomedical engineering. He has published six papers in international journals and three in international conferences.

Mr. Antipas received the Thomaidio foundation, (NTUA) award in 2003 and 2004. He is the recipient of a scholarship from the Diagnostic and Therapeutic Center of Athens "Hygeia/Harvard Medical International" in 2003, and "HERAKLEITOS" in 2004.



Nikolaos K. Uzunoglu (M'82–SM'97–F'06) was born in Constantinople, Turkey, in 1951. He received the B.Sc. degree in electrical engineering from the Istanbul Technical University, Istanbul, Turkey, in 1973. He received the M.Sc. and Ph.D. degrees from the University of Essex, Essex, U.K., in 1974 and 1976, respectively.

He worked for the Hellenic Navy Research and Development Office from 1977 to 1984. In 1984, he was elected Associate Professor in the Department of Electrical and Computer Engineering (DECE), the National Technical University of Athens (NTUA), Athens, Greece. He served as Dean of the DECE for six years and Director of the Institute of Communication and Computer Systems of NTUA for eight years. He is the Head of the Microwave and Fibre Optics Laboratory, DECE, NTUA, which is actively engaged among other fields in oncologic research. He has been the project manager of several European Commission projects (e.g., FRANS/ACTS, EUROMED/DGIII, and NEW ROENTGEN/IST). He has published more than 150 journal articles, one international book (editor), three books in Greek and has made numerous conference contributions. His research interests include electromagnetic theory, microwaves, fibre optics, telecommunications, biomedical engineering, and *in silico* oncology.

In 1981, Dr. Uzunoglu received the International G. Marconi Award in Telecommunications. He is a member of the Academy of Sciences of Armenia.